

NATIONAL INSTITUTE FOR FUSION SCIENCE

Collisionless Driven Magnetic Reconnection

R. Horiuchi and T. Sato

(Received – June 3, 1993)

NIFS-233

June 1993

RESEARCH REPORT NIFS Series

This report was prepared as a preprint of work performed as a collaboration research of the National Institute for Fusion Science (NIFS) of Japan. This document is intended for information only and for future publication in a journal after some rearrangements of its contents.

Inquiries about copyright and reproduction should be addressed to the Research Information Center, National Institute for Fusion Science, Nagoya 464-01, Japan.

COLLISIONLESS DRIVEN MAGNETIC RECONNECTION

Ritoku Horiuchi and Tetsuya Sato

National Institute for Fusion Science,

Nagoya 464-01, Japan

Abstract

Driven magnetic reconnection in a collisionless plasma is investigated by means of a two-and-one-half dimensional particle simulation. The dynamical compression by plasma inflow forms a peaked profile of current density in the neutral sheet. When the width of current layer is compressed as thin as the ion Larmor radius, the charge separation becomes distinct abruptly at the center of the current layer due to the finite ion Larmor radius effect. The charge separation in the central current region and the subsequent spatial modification of the current profile result in excitation of collisionless driven magnetic reconnection. In the cause of collisionless driven magnetic reconnection an efficient energy conversion from field energy to particle energy is observed.

Keywords; driven magnetic reconnection, finite Larmor effect, collisionless plasma, particle simulation, energy conversion

Magnetohydrodynamic (MHD) studies^{1),2)} have disclosed that driven magnetic reconnection plays an essential role on the energy relaxation and the self-organization of a magnetically confined plasma. Under the influence of a driving source and a small amount of electrical resistivity, magnetic reconnection takes place in a time scale much shorter than the resistive time scale and the reconnection rate is primarily determined by the driving electric field.³⁾ This process can lead to fast energy conversion from the field energy to the particle energy as well as a topological change of magnetic field.¹⁾⁻³⁾ On the other hand, energetically active phenomena⁴⁾ triggered by magnetic reconnection are often observed in a high temperature, rarefied plasma in which binary collisions between particles are negligible, namely, in a collisionless plasma. It is not so easy to explain how an electric field along the equilibrium current is generated in the neutral sheet of collisionless plasma. The concept of an anomalous resistivity⁵⁾ which originates from the wave-particle interaction or the stochasticity of particle orbit has been introduced to explain collisionless reconnection. But this is not confirmed in a self-consistent manner. Leboeuf et al.⁶⁾ and Hewett et al.⁷⁾ have also examined the collisionless magnetic reconnection by means of particle simulation. However, some of the assumptions done by them are not appropriate for the analysis of driven magnetic reconnection. Especially, it is quite important to describe the displacement current and a finite ion Larmor radius effect in the current layer in a self-consistent manner, as will be shown in this paper. The purpose of this letter is then to demonstrate the dynamical evolution of driven magnetic reconnection in a collisionless plasma by means of particle simulation and to clarify the mechanism leading to the excitation of driven magnetic reconnection and to the resultant fast energy conversion.

By solving the equations of motion and the Maxwell equations in a self-consistent manner we examine the dynamical evolution of physical quantities in an open system. Our code is two-and-one-half dimensional particle code which relies on the semi-implicit

method.⁸⁾⁻¹⁰⁾ Physical quantities are assumed to have a translational symmetry along the z -axis in the Cartesian coordinates (x, y, z) . As an initial condition we adopt one dimensional Harris-type equilibrium with a magnetically neutral sheet along the mid-horizontal line ($y = 0$) as

$$B_x(y) = B_0 \tanh(y/L), \quad (1)$$

$$P(y) = B_0^2/8\pi \operatorname{sech}^2(y/L), \quad (2)$$

where L is the scale height along the y -axis. Since both an ion and an electron are loaded at the same spatial position, there should be no electric field in the initial profile. Particle temperature is assumed to be spatially uniform and isotropic. In order to drive magnetic reconnection at the center of simulation domain we adopt a free boundary condition,⁹⁾ under which the plasma is smoothly supplied by an $\mathbf{E} \times \mathbf{B}$ drift from two input boundaries ($y = \pm y_b$), and the reconnected plasma can flow out smoothly through two output boundaries ($x = \pm x_b$). The ratio x_b/y_b of the side lengths of the simulation domain is fixed to 3 in this study. The driving electric field at the input boundaries $\mathbf{E}(x, t) = (0, 0, E_{ex}(x, t))$ is initially zero and gradually increases until it reaches to a constant value. The spatial profile of $E_{ex}(x, t)$ is determined so that the input flow velocity becomes maximum at the mid-point ($x = 0$) of the input boundary. The maximum input velocity is fixed to 0.5 of the initial average Alfvén velocity v_A . The total number of particles used here is 240,000 and the ratio of ion to electron mass is 50. The initial average ion Larmor radius is about 7.5 of a grid separation distance Δy along the y -direction, which is smaller than the scale height of the current profile $L (= 12.6\Delta y)$. The collisionless skin depth δ_s ($= c/\omega_{pe}$) is equal to Δy , where ω_{pe} is the average electron plasma frequency.¹¹⁾

Figure 1 shows five snapshots of magnetic flux contours (left) and vector plots of the average ion velocity (right) where the top, the second, the third, the fourth and the bottom panels correspond to the profiles at $t = 0$, $t = 0.56t_A$, $t = 1.12t_A$, $t = 1.68t_A$ and

$t = 2.24t_A$, respectively. Here, time is measured by the Alfvén transit time $t_A (= 2y_b/v_A)$ along the y -axis, and the magnetic flux contours less than the values at the mid-point ($x = 0, y = 0$) are plotted by the dotted line. A magnetically neutral sheet exists along the mid-horizontal line and no bulk ion flow is in the (x, y) plane at initial (top panel). Time proceeds from the top to the bottom in this figure. Magnetic reconnection sets in and an x-shaped structure of magnetic separatrix is formed at the period of $t \approx t_A$. The region occupied by the reconnected flux spreads over the whole simulation domain at this time. A fast directed flow arises from the x-point as a result of magnetic reconnection and it carries the reconnected flux toward the open boundaries. One can find in the bottom panel that the shock structure appears in the ion flow pattern.

Let us examine the reconnection process in more detail. Figures 2(a) and 2(b) show (a) the time histories of the z -components of the average electron velocity (solid line) and the average ion velocity (dotted line), and (b) those of the y -components of the electron thermal velocity (solid line) and the ion thermal velocity (dotted line) where the average velocities are observed at the x-point, and the thermal velocities are observed at the downstream side of the x-point. The equilibrium current is initially dominated by the diamagnetic component. The converging plasma flow creates a peaked profile for the mass density and current density as time goes on. Because the ions take a slightly broader spatial distribution than that of electrons due to the finite ion Larmor radius effect, the charge separation takes place along the density gradient and hence an electric field appears in the y direction. The resultant $\mathbf{E} \times \mathbf{B}$ drift has the same sign as the electron diamagnetic drift. Thus, the electron current becomes dominant over the ion current, as was shown in Fig. 2(a). The ion thermal velocity increases slowly in the initial compression phase, while the electron thermal velocity remains almost constant. As magnetic reconnection sets in, the electron thermal velocity increases suddenly. This phenomenon suggests that electron heating takes place actively through collisionless reconnection.

What is the trigger of magnetic reconnection in a collisionless plasma ? Figures 3(a) and 3(b) show (a) the time histories of the half-width l_h of the mass density profile (solid line) and the ion Larmor radius λ_i (dotted line), and (b) those of the electron number density (solid line) and the ion number density (dotted line) at the x-point where the ion Larmor radius is defined by using the ion thermal velocity in the current layer and the magnetic field outside the current layer. In the vicinity of the magnetically neutral sheet an ion executes a meandering motion¹⁰⁾ with the orbit amplitude of $l_m \approx \sqrt{l_h \lambda_i}$. The ion motion is free from magnetic field in the inner region ($r \leq l_m$) of the current layer. The mass density profile has initially the width about two times larger than the ion Larmor radius. The width l_h decreases with time faster than the ion Larmor radius λ_i . When l_h becomes nearly equal to λ_i , both l_h and λ_i tend to change slowly with the same rate. In other words, the current layer evolves slowly while keeping the width nearly equal to the ion Larmor radius after this period ($t > t_A$). This result is quite different from that of the numerical simulation done by Hewett et al..⁷⁾ The number density at the x-point begins to increase at $t \approx 0.5t_A$. Both the electron density and the ion density increase with the same growth rate during the period of $0.5t_A < t < t_A$. After this period the growth of the number density slows down and the electron density becomes dominant over the ion density. Comparing Fig. 3(a) with Fig. 3(b), one can find that the charge separation becomes distinct after the width of the current layer becomes nearly equal to the ion Larmor radius. This phenomenon can be easily understood by the finite ion Larmor radius effect in the vicinity of the neutral sheet. That is, most of the ions in the current layer become unmagnetized when $l_h \approx \lambda_i$, while the electrons remain magnetized. Therefore, the compression by the input flow does not work on the ions but only on the electrons in the current layer. Consequently, the charge neutrality condition is violated in the central region of the current layer after this period. Note that this period is in good agreement with the starting time of magnetic reconnection and the width of the

current layer in the reconnection phase is much larger than that of the Rosenbluth sheath $\delta(= (M_e/M_i)^{1/2} \lambda_i)$.¹¹⁾

Generation of electric field along the equilibrium current is needed for excitation of magnetic reconnection. Figures 4(a) and 4(b) show (a) the z -component of the electric field $|E_z|$ at the x -point versus time in the unit of the Alfvén transit time and (b) that of the current density $|J_z|$ at the x -point. Note that the electric field is plotted in the logarithmic scale, while the current density is plotted in the linear scale. The current density J_z grows gradually in the compression time scale while the electric field E_z remains at the noise level until magnetic reconnection starts ($t < t_A$). The electric field begins to grow as soon as magnetic reconnection sets in ($t \approx t_A$). The inclination of the growth curve becomes steeper as time goes on. The growth rate is estimated to be $5/t_A$ in the first phase of reconnection and $20/t_A$ in the later phase. It is worthy to note that the growth time is roughly explained by the compression time scale $t_c(= l_h/(0.5v_A))$ of the current layer which is nearly equal to the traveling time of the thermal electron over the charge separation zone along the x -axis. The generation of the electric field means that the constant acceleration of the electrons in the current layer by the electric field is requisite for keeping the equilibrium current. In other words, the electrons which carry the equilibrium current are constantly supplied into and move away from the current layer. Accordingly, the ratio of the electric field to the current density, which can be interpreted as representing an effective resistivity, is roughly estimated by introducing a correlation time.¹²⁾ If we take the compression time scale $l_h/(0.5v_A)$ as a correlation time, the normalized effective resistivity $\tilde{\eta}$ is estimated to $4\pi\omega_{ce}/\omega_{pe}^2 t_c \approx 3 \cdot 10^{-3}$ in our case. This value is in good agreement with the observed value ($10^{-3} < \tilde{\eta}_{obs} < 5 \cdot 10^{-3}$).

Let us examine the mechanism that generates the neutral sheet electric field along the equilibrium current and excites magnetic reconnection, in connection with the charge separation in the central region of the current layer. The charge separation generates

the convergent electric field around the mid-point along the neutral sheet in the (x, y) plane. The y -component of the electric field, E_y , increases slowly while satisfying the force balance with the dynamic compression for the electrons. On the other hand, there is no such counter force in the x direction. Therefore, the convergent electric field resultantly pushes the electrons in the central region of the neutral sheet away from the center in the x direction, thus modifying the spatial distribution of the equilibrium current, the great part of which is carried by electrons (see Fig. 2(a)). The displacement current responds quickly to this modification and works to keep the equilibrium current in the central region of the neutral sheet. The neutral sheet electric field E_z along the equilibrium current is thus created by the displacement current. This can explain the observational fact that the growth time of the E_z field is roughly represented by the compression time scale $l_h/(0.5v_A)$ of the current layer and that the growth time is also equal to the traveling time of the thermal electron over the charge separation zone.

From this consideration we can come to the conclusion that collisionless reconnection is triggered under the influence of a converging driving flow and that a dc type electric field leading to reconnection is created by the displacement current originated from the finite ion Larmor radius effect, instead of the wave-particle interaction induced resistivity.

The E_z field not only acts to accelerate electrons along the z -axis but also results in reconnecting magnetic field lines. Consequently, the y -component of magnetic field B_y appears along the neutral sheet in accordance with the growth of the E_z field. Figures 5(a) and 5(b) show (a) the spatial distribution of the y -component of the magnetic field B_y along the neutral sheet at $t = 2.02t_A$ and (b) that of the electron temperature T_e where the electron temperature is estimated by assuming that the electron distribution can be approximated by the shifted Maxwellian. The B_y field grows on both sides of the reconnection point along the mid-horizontal line. Electrons accelerated along the x direction by the electric field E_x are quickly trapped by the B_y field and thus it appears

that the electrons are thermalized. Comparing Fig. 5(a) with Fig. 5(b), one can find that the electron heating takes place most efficiently at the downstream side of the reconnection point. This result is consistent with the observation that the electron thermal velocity at the downstream side increases rapidly, say, by factor 5, as magnetic reconnection sets in (Fig 2(b)). In this way the energy conversion from the field energy to the particle energy is realized through collisionless driven magnetic reconnection.

One of the authors (R.H.) is grateful to Professors W. Horton and T. Tajima for their interests in this work.

References

1. R. Horiuchi and T. Sato, Phys. Rev. Lett. **55**, 211(1985); R. Horiuchi and T. Sato, Phys. Fluids **29**, 1161, 4174(1986), 1142(1988).
2. T. Sato, Y. Nakayama, T. Hayashi, K. Watanabe, and R. Horiuchi, Phys. Rev. Lett. **63**, 528(1989); M. Yamada, Y. Ono, A. Hayakawa, M. Katsurai, and F. W. Perkins, Phys. Rev. Lett. **65**, 721(1990); R. Horiuchi and T. Sato, Phys. Fluids B **4**, 672(1992).
3. T. Sato and T. Hayashi, Phys. Fluids **22**, 1189(1979); T. Sato, T. Hayashi, K. Watanabe, R. Horiuchi, M. Tanaka, N. Sawairi and K. Kusano, Phys. Fluids B **4**, 450(1992).
4. E. R. Priest, *Solar Magnetohydrodynamics* (Dordrecht,Reidel,1982); A. Nishida, *Geomagnetic Diagnostics of the Magnetosphere* (Springer-Verlang, New York, 1978); A. Hasegawa and T. Sato, *Space Plasma Physics 1* (Springer-Verlang, New York, 1989).

5. R. C. Davidson and N. T. Gladd, *Phys. Fluids* **18**, 1327(1975); A. A. Galeev and L. M. Zelenyi, *Sov. Phys. JETP* **43**, 1113(1976); A. A. Galeev, *Basic Plasma Physics II* (North-Holland Physics Publishing, New York, 1984), p.305.
6. J. N. Leboeuf, T. Tajima and J. M. Dawson, *Phys. Fluids* **25**, 784(1982).
7. D. W. Hewett, G. E. Frances and C. E. Max, *Phys. Rev. Lett.* **61**, 893(1988).
8. M. Tanaka and T. Sato, *Phys. Fluids* **29**, 3823(1986).
9. S. Murakami and T. Sato, *J. Phys. Soc. Japan* **61**, 849(1992).
10. R. Horiuchi and T. Sato, *Phys. Fluids B* **2**, 2652(1990).
11. M. N. Rosenbluth, *Magnetohydrodynamics : A Symposium* (Stanford University, Stanford, 1957), Vol. 1, p. 62; M. G. Haines, *Nucl. Fusion* **17**, 811(1977).
12. W. Horton and T. Tajima, *Geophys. Res. Lett.* **17**, 123(1990).

Figure captions

Fig. 1. Magnetic flux contours (left) and vector plots of average ion velocity (right) at five different time periods where five panels correspond to the profiles at $t = 0, 0.56t_A, 1.12t_A, 1.68t_A$, and $t = 2.24t_A$, respectively.

Fig. 2. (a) Time histories of the z -components of average electron velocity (solid line) and average ion velocity (dotted line) at the x-point, and (b) those of the y -components of the electron thermal velocity (solid line) and the ion thermal velocity (dotted line) at the downstream side of the x-point where the thermal velocities are plotted in the logarithmic scale and the average velocities are plotted in the linear scale.

Fig. 3. (a) Time histories of the half-width l_h of the mass density profile (solid line) and the ion Larmor radius λ_i (dotted line), and (b) those of the electron number density (solid line) and the ion number density (dotted line) at the x-point where the ion Larmor radius is defined by using the ion thermal velocity in the current layer and the magnetic field outside the current layer.

Fig. 4. (a) The z -component of the electric field $|E_z|$ at the x-point versus the time normalized by the Alfvén transit time and (b) that of the current density $|J_z|$. Notice that the electric field is plotted in the logarithmic scale while the current density is plotted in the linear scale.

Fig. 5. (a) Spatial distribution of the y -component of magnetic field B_y along the neutral sheet at $t = 2.02t_A$ and (b) that of the electron temperature T_e .

Figure 1

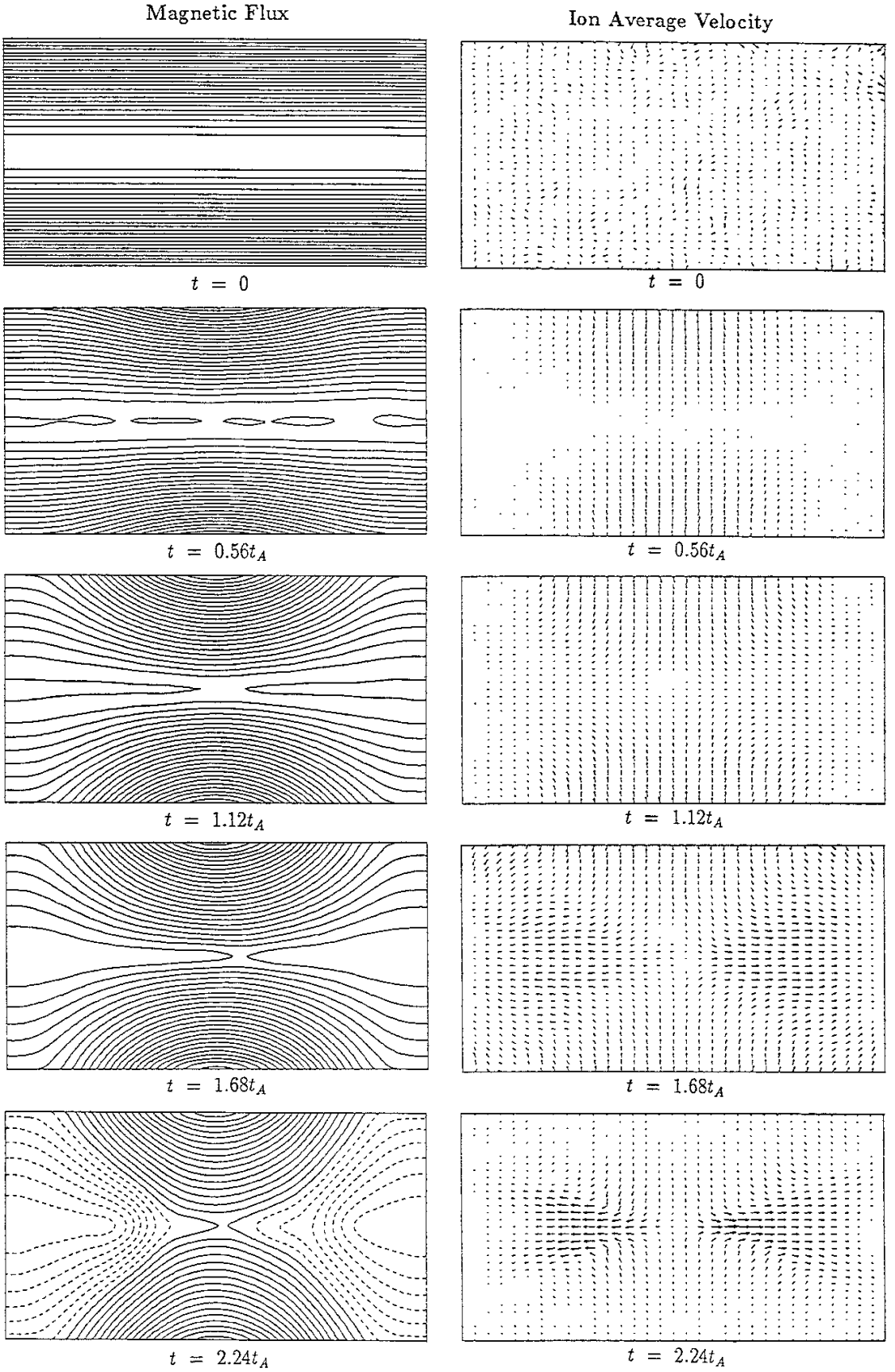


Figure 2

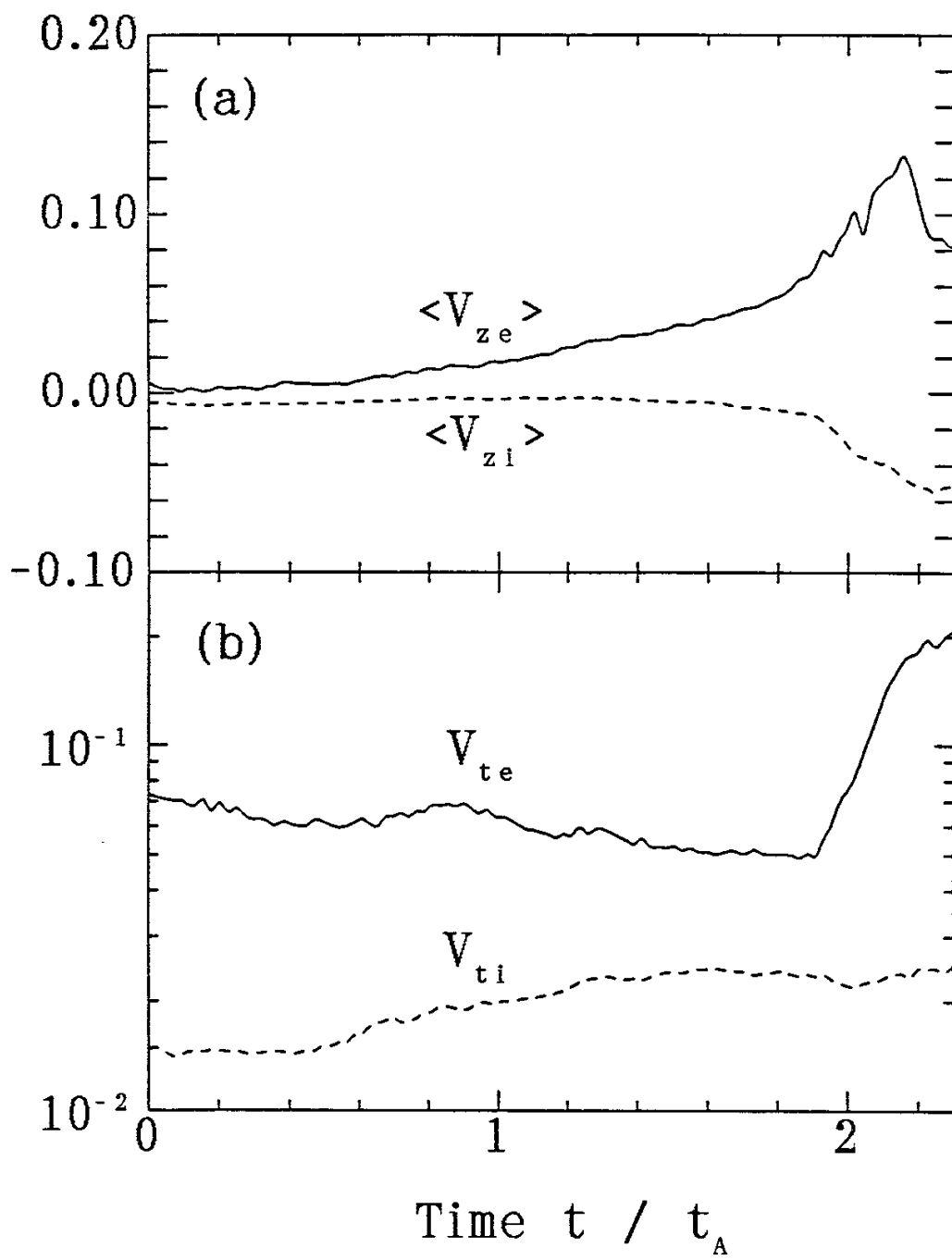


Figure 3

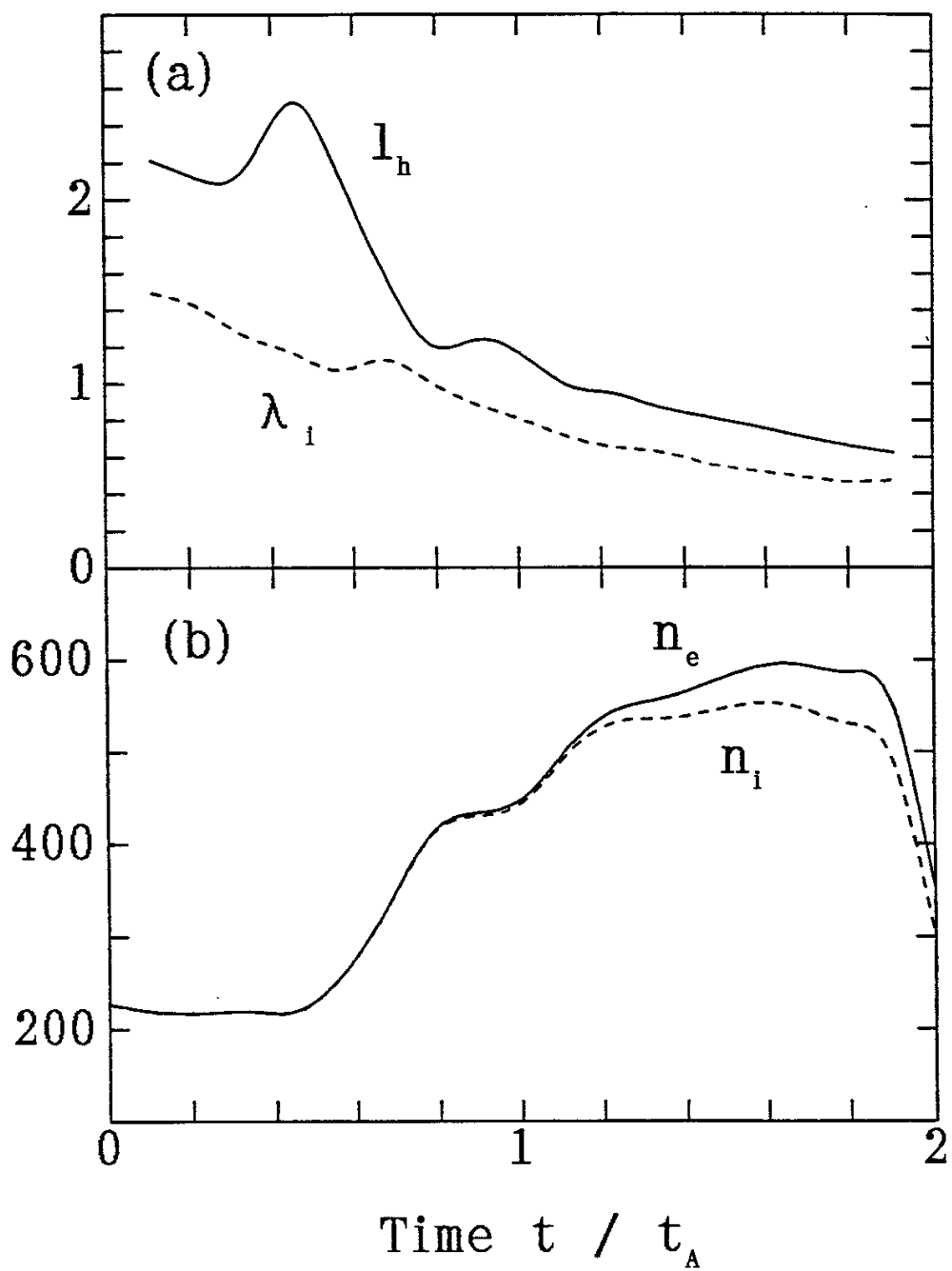


Figure 4

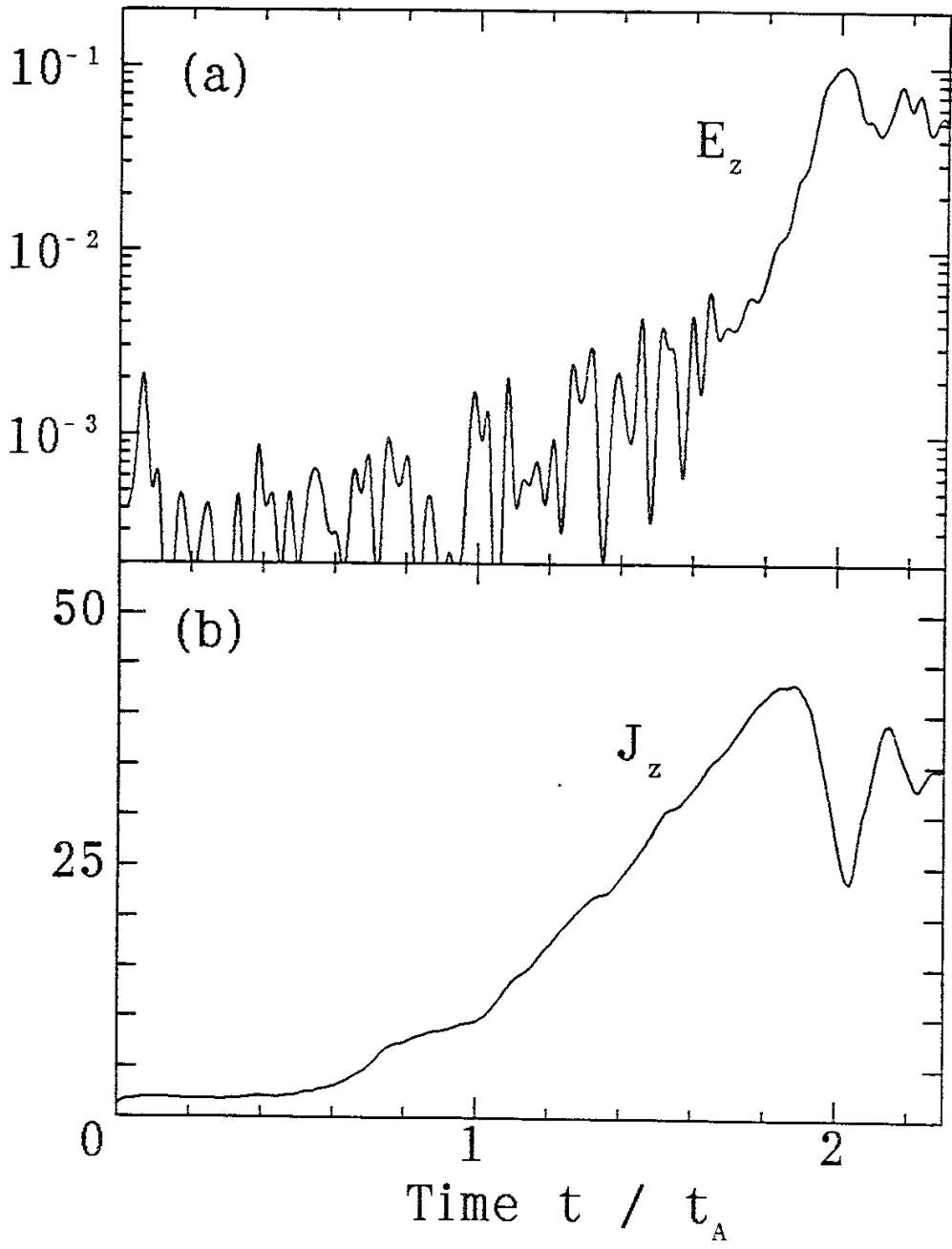
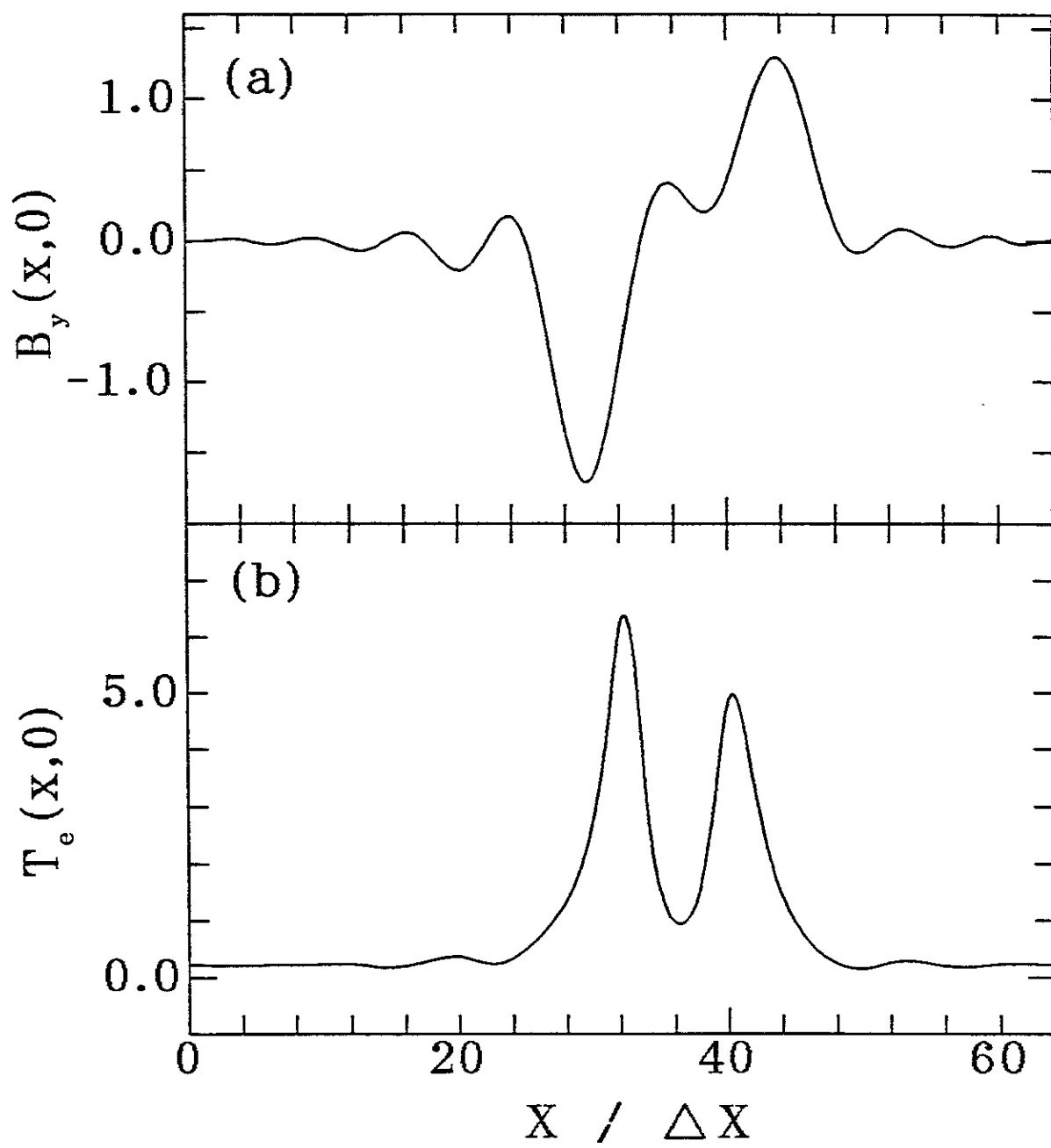


Figure 5



Recent Issues of NIFS Series

- NIFS-185 H. Yamada, S. Morita, K. Ida, S. Okamura, H. Iguchi, S. Sakakibara, K. Nishimura, R. Akiyama, H. Arimoto, M. Fujiwara, K. Hanatani, S. P. Hirshman, K. Ichiguchi, H. Idei, O. Kaneko, T. Kawamoto, S. Kubo, D. K. Lee, K. Matsuoka, O. Motojima, T. Ozaki, V. D. Pustovitov, A. Sagara, H. Sanuki, T. Shoji, C. Takahashi, Y. Takeiri, Y. Takita, S. Tanahashi, J. Todoroki, K. Toi, K. Tsumori, M. Ueda and I. Yamada, *MHD and Confinement Characteristics in the High- β Regime on the CHS Low-Aspect-Ratio Heliotron / Torsatron* ; Sep. 1992
- NIFS-186 S. Morita, H. Yamada, H. Iguchi, K. Adati, R. Akiyama, H. Arimoto, M. Fujiwara, Y. Hamada, K. Ida, H. Idei, O. Kaneko, K. Kawahata, T. Kawamoto, S. Kubo, R. Kumazawa, K. Matsuoka, T. Morisaki, K. Nishimura, S. Okamura, T. Ozaki, T. Seki, M. Sakurai, S. Sakakibara, A. Sagara, C. Takahashi, Y. Takeiri, H. Takenaga, Y. Takita, K. Toi, K. Tsumori, K. Uchino, M. Ueda, T. Watari, I. Yamada, *A Role of Neutral Hydrogen in CHS Plasmas with Reheat and Collapse and Comparison with JIPP T-IIU Tokamak Plasmas* ; Sep. 1992
- NIFS-187 K. Itoh, S.-I. Itoh, A. Fukuyama, M. Yagi and M. Azumi, *Model of the L-Mode Confinement in Tokamaks* ; Sep. 1992
- NIFS-188 K. Itoh, A. Fukuyama and S.-I. Itoh, *Beta-Limiting Phenomena in High-Aspect-Ratio Toroidal Helical Plasmas*; Oct. 1992
- NIFS-189 K. Itoh, S. -I. Itoh and A. Fukuyama, *Cross Field Ion Motion at Sawtooth Crash* ; Oct. 1992
- NIFS-190 N. Noda, Y. Kubota, A. Sagara, N. Ohyabu, K. Akaishi, H. Ji, O. Motojima, M. Hashiba, I. Fujita, T. Hino, T. Yamashina, T. Matsuda, T. Sogabe, T. Matsumoto, K. Kuroda, S. Yamazaki, H. Ise, J. Adachi and T. Suzuki, *Design Study on Divertor Plates of Large Helical Device (LHD)* ; Oct. 1992
- NIFS-191 Y. Kondoh, Y. Hosaka and K. Ishii, *Kernel Optimum Nearly-Analytical Discretization (KOND) Algorithm Applied to Parabolic and Hyperbolic Equations* : Oct. 1992
- NIFS-192 K. Itoh, M. Yagi, S.-I. Itoh, A. Fukuyama and M. Azumi, *L-Mode Confinement Model Based on Transport-MHD Theory in Tokamaks* ; Oct. 1992
- NIFS-193 T. Watari, *Review of Japanese Results on Heating and Current Drive* ; Oct. 1992

- NIFS-194 Y. Kondoh, *Eigenfunction for Dissipative Dynamics Operator and Attractor of Dissipative Structure* ; Oct. 1992
- NIFS-195 T. Watanabe, H. Oya, K. Watanabe and T. Sato, *Comprehensive Simulation Study on Local and Global Development of Auroral Arcs and Field-Aligned Potentials* ; Oct. 1992
- NIFS-196 T. Mori, K. Akaishi, Y. Kubota, O. Motojima, M. Mushiaki, Y. Funato and Y. Hanaoka, *Pumping Experiment of Water on B and LaB₆ Films with Electron Beam Evaporator* ; Oct., 1992
- NIFS-197 T. Kato and K. Masai, *X-ray Spectra from Hinotori Satellite and Suprathermal Electrons* ; Oct. 1992
- NIFS-198 K. Toi, S. Okamura, H. Iguchi, H. Yamada, S. Morita, S. Sakakibara, K. Ida, K. Nishimura, K. Matsuoka, R. Akiyama, H. Arimoto, M. Fujiwara, M. Hosokawa, H. Idei, O. Kaneko, S. Kubo, A. Sagara, C. Takahashi, Y. Takeiri, Y. Takita, K. Tsumori, I. Yamada and H. Zushi, *Formation of H-mode Like Transport Barrier in the CHS Heliotron / Torsatron* ; Oct. 1992
- NIFS-199 M. Tanaka, *A Kinetic Simulation of Low-Frequency Electromagnetic Phenomena in Inhomogeneous Plasmas of Three-Dimensions* ; Nov. 1992
- NIFS-200 K. Itoh, S.-I. Itoh, H. Sanuki and A. Fukuyama, *Roles of Electric Field on Toroidal Magnetic Confinement*, Nov. 1992
- NIFS-201 G. Gnudi and T. Hatori, *Hamiltonian for the Toroidal Helical Magnetic Field Lines in the Vacuum*; Nov. 1992
- NIFS-202 K. Itoh, S.-I. Itoh and A. Fukuyama, *Physics of Transport Phenomena in Magnetic Confinement Plasmas*; Dec. 1992
- NIFS-203 Y. Hamada, Y. Kawasumi, H. Iguchi, A. Fujisawa, Y. Abe and M. Takahashi, *Mesh Effect in a Parallel Plate Analyzer*; Dec. 1992
- NIFS-204 T. Okada and H. Tazawa, *Two-Stream Instability for a Light Ion Beam-Plasma System with External Magnetic Field*; Dec. 1992
- NIFS-205 M. Osakabe, S. Itoh, Y. Gotoh, M. Sasao and J. Fujita, *A Compact Neutron Counter Telescope with Thick Radiator (Cotetra) for Fusion Experiment*; Jan. 1993
- NIFS-206 T. Yabe and F. Xiao, *Tracking Sharp Interface of Two Fluids by the CIP (Cubic-Interpolated Propagation) Scheme*, Jan. 1993

- NIFS-207 A. Kageyama, K. Watanabe and T. Sato, *Simulation Study of MHD Dynamo : Convection in a Rotating Spherical Shell*; Feb. 1993
- NIFS-208 M. Okamoto and S. Murakami, *Plasma Heating in Toroidal Systems*; Feb. 1993
- NIFS-209 K. Masai, *Density Dependence of Line Intensities and Application to Plasma Diagnostics*; Feb. 1993
- NIFS-210 K. Ohkubo, M. Hosokawa, S. Kubo, M. Sato, Y. Takita and T. Kuroda, *R&D of Transmission Lines for ECH System* ; Feb. 1993
- NIFS-211 A. A. Shishkin, K. Y. Watanabe, K. Yamazaki, O. Motojima, D. L. Grekov, M. S. Smirnova and A. V. Zolotukhin, *Some Features of Particle Orbit Behavior in LHD Configurations*; Mar. 1993
- NIFS-212 Y. Kondoh, Y. Hosaka and J.-L. Liang, *Demonstration for Novel Self-organization Theory by Three-Dimensional Magnetohydrodynamic Simulation*; Mar. 1993
- NIFS-213 K. Itoh, H. Sanuki and S.-I. Itoh, *Thermal and Electric Oscillation Driven by Orbit Loss in Helical Systems*; Mar. 1993
- NIFS-214 T. Yamagishi, *Effect of Continuous Eigenvalue Spectrum on Plasma Transport in Toroidal Systems*; Mar. 1993
- NIFS-215 K. Ida, K. Itoh, S.-I. Itoh, Y. Miura, JFT-2M Group and A. Fukuyama, *Thickness of the Layer of Strong Radial Electric Field in JFT-2M H-mode Plasmas*; Apr. 1993
- NIFS-216 M. Yagi, K. Itoh, S.-I. Itoh, A. Fukuyama and M. Azumi, *Analysis of Current Diffusive Ballooning Mode*; Apr. 1993
- NIFS-217 J. Guasp, K. Yamazaki and O. Motojima, *Particle Orbit Analysis for LHD Helical Axis Configurations* ; Apr. 1993
- NIFS-218 T. Yabe, T. Ito and M. Okazaki, *Holography Machine HORN-1 for Computer-aided Retrieve of Virtual Three-dimensional Image* ; Apr. 1993
- NIFS-219 K. Itoh, S.-I. Itoh, A. Fukuyama, M. Yagi and M. Azumi, *Self-sustained Turbulence and L-Mode Confinement in Toroidal Plasmas* ; Apr. 1993
- NIFS-220 T. Watari, R. Kumazawa, T. Mutoh, T. Seki, K. Nishimura and F. Shimpo, *Applications of Non-resonant RF Forces to Improvement of Tokamak Reactor Performances Part I: Application of Ponderomotive Force* ; May 1993

- NIFS-221 S.-I. Itoh, K. Itoh, and A. Fukuyama, *ELMy-H mode as Limit Cycle and Transient Responses of H-modes in Tokamaks* ; May 1993
- NIFS-222 H. Hojo, M. Inutake, M. Ichimura, R. Katsumata and T. Watanabe, *Interchange Stability Criteria for Anisotropic Central-Cell Plasmas in the Tandem Mirror GAMMA 10* ; May 1993
- NIFS-223 K. Itoh, S.-I. Itoh, M. Yagi, A. Fukuyama and M. Azumi, *Theory of Pseudo-Classical Confinement and Transmutation to L-Mode*; May 1993
- NIFS-224 M. Tanaka, *HIDENEK: An Implicit Particle Simulation of Kinetic-MHD Phenomena in Three-Dimensional Plasmas*; May 1993
- NIFS-225 H. Hojo and T. Hatori, *Bounce Resonance Heating and Transport in a Magnetic Mirror*; May 1993
- NIFS-226 S.-I. Itoh, K. Itoh, A. Fukuyama, M. Yagi, *Theory of Anomalous Transport in H-Mode Plasmas*; May 1993
- NIFS-227 T. Yamagishi, *Anomalous Cross Field Flux in CHS* ; May 1993
- NIFS-228 Y. Ohkouchi, S. Sasaki, S. Takamura, T. Kato, *Effective Emission and Ionization Rate Coefficients of Atomic Carbons in Plasmas*; June 1993
- NIFS-229 K. Itoh, M. Yagi, A. Fukuyama, S.-I. Itoh and M. Azumi, *Comment on 'A Mean Field Ohm's Law for Collisionless Plasmas*; June 1993
- NIFS-230 H. Idei, K. Ida, H. Sanuki, H. Yamada, H. Iguchi, S. Kubo, R. Akiyama, H. Arimoto, M. Fujiwara, M. Hosokawa, K. Matsuoka, S. Morita, K. Nishimura, K. Ohkubo, S. Okamura, S. Sakakibara, C. Takahashi, Y. Takita, K. Tsumori and I. Yamada, *Transition of Radial Electric Field by Electron Cyclotron Heating in Stellarator Plasmas*; June 1993
- NIFS-231 H.J. Gardner and K. Ichiguchi, *Free-Boundary Equilibrium Studies for the Large Helical Device*, June 1993
- NIFS-232 K. Itoh, S.-I. Itoh, A. Fukuyama, H. Sanuki and M. Yagi, *Confinement Improvement in H-Mode-Like Plasmas in Helical Systems*, June 1993